ISSN 1097-0002

TXRF FOR SEMICONDUCTOR APPLICATIONS

Yoshihiro Mori*

Advanced Technology Research Laboratories, Nippon Steel Corporation
c/o Wacker-NSCE Corporation, 3434 Shimata, Hikari, Yamaguchi 743-0063, Japan

ABSTRACT

This paper discusses the application of TXRF for semiconductor process characterization. The depth profile of the analyte element plays a critical role in accurate determination by TXRF. In order to achieve reliable quantification, a method for preparing standard and crosscheck samples, named "Immersion in Alkaline Hydrogen Peroxide Solution (IAP)," is proposed. The method offers a good level of reproducibility of depth profiles as well as areal and in-batch uniformity. Certain improvements of TXRF instruments are also discussed. The purity of the background spectra is critical in ultra-trace analysis, and improvements in instrumentation such as Au-Lβ excitation, a dual multilayer monochromator, and an *x-y-θ* stage actually reduced the background to help enable the identification of trace elements. We tested the performance of the recently improved TXRF instruments on IAP wafers intentionally contaminated with trace Cu, and demonstrated that a real-10^9 atoms cm^{-2} analysis can actually be achieved.

1. INTRODUCTION

In the semiconductor industry at present, control of contamination is a critical element in stabilizing yield. For metallic contamination, many analytical tools such as Vapor Phase Decomposition - Atomic Absorption Spectrophotometry (VPD-AAS), VPD - Inductively Coupled Plasma - Mass Spectrometry (VPD-ICP-MS) [1], and Total-reflection X-Ray Fluorescence Spectrometry (TXRF) are currently used for process characterization. In recent methods of semiconductor processing, large-diameter wafers such as 300-mmϕ wafers are becoming increasingly popular, and many single-wafer processes are being introduced instead of the traditional batch processes. Accordingly, localized contamination occurs more frequently, meaning that the mapping capabilities of analytical techniques are becoming increasingly important. TXRF is the only tool that can nondestructively map surface metal contamination at a high degree of sensitivity [2]. In addition, many new metals such as Cu, Co, and Ru are being used or tested as alternative materials. Since their cross-contamination is critical in the properties of Large Scale Integration (LSI) devices, the number of metal species requiring control is increasing. TXRF is suitable for analyzing such elements as well,

* *Present affiliation: R&D Group, Wacker-NSCE Corporation*
3434 Shimata, Hikari, Yamaguchi 743-0063, Japan

ISSN 1097-0002

This document was presented at the Denver X-ray Conference (DXC) on Applications of X-ray Analysis.

Sponsored by the International Centre for Diffraction Data (ICDD).

This document is provided by ICDD in cooperation with the authors and presenters of the DXC for the express purpose of educating the scientific community.

Usage is restricted for the purposes of education and scientific research.

DXC Website
– www.dxcicdd.com

ICDD Website
- www.icdd.com

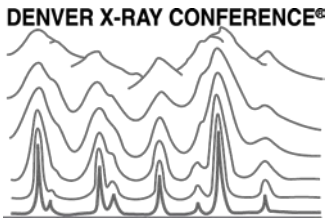

ISSN 1097-0002

because it can analyze many elements simultaneously. Because of these positive characteristics, almost all leading-edge semiconductor manufacturers have introduced TXRF machines for contamination control.

TXRF is actually a very powerful tool for rapid qualitative analysis, but the implementation of accurate quantitative analysis by TXRF is not without some problems because of many error factors [3]. The error factors can be classified into two major groups, those related to the samples and those related to the instruments. The sample factors include items such as lateral distribution and depth profile of the analyte; the instrument-related factors include mechanical precision, purity of background spectra, and so on. In this paper, we focus on the issues of depth profile and the purity of background spectra, as representatives of the two groups. In discussing the first issue, we will examine the impact of depth profile to fluorescent X-ray intensity, propose a method to prepare standard samples for TXRF, and examine the applicability of the samples to calibration and cross-checking. Then, in discussing the second issue, we will introduce recent improvements in TXRF instruments. Finally, based on these two technologies, we will experimentally examine the performance of recently improved TXRF machines as used for the control of contamination in semiconductor fabrication processes.

2. STANDARD SAMPLE ISSUE

2-1. Effect of depth profile

The fluorescent X-ray intensity in TXRF is highly sensitive to the depth profile of the analyte. Figure 1 schematically demonstrates this fact. Two types of depth profiles are assumed: (a) near-surface analyte and (b) implanted analyte. The amount of analyte is assumed to be the same. Since the substrate absorbs the penetrated primary X-rays, exponential attenuation occurs along the depth, as illustrated in the figures on the left. The intensity of the fluorescent X-ray is proportional to the integration of the product of concentration and excitation X-ray intensity along the depth, which is illustrated in the figures on the right. The difference of the areas explicitly indicates that different depth profiles give different fluorescent X-ray intensities even though the amount of analyte is the same.

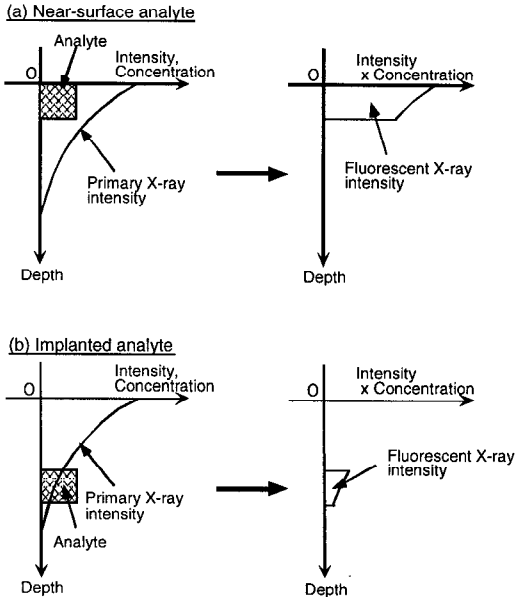

Fig. 1 Schematic illustrations explaining the differences in the intensity of X-ray fluorescence for two types of analytes with different depth profiles.

We actually found some examples of the effect of depth profile for TXRF in standard samples. Figure 2 shows the anglescans of two spincoat [4] standard samples prepared by following the

ISSN 1097-0002

same process. Although their targeted concentrations were the same, 5 x 10^{13} atoms cm^{-2}, their anglescans were apparently different. At 0.10 deg., which is the typical measurement angle in actual use, the difference in fluorescent X-ray intensity is more than double. Similar differences were observed for standard microdrop [5] samples as well. In spincoat or microdrop samples, metals physically adsorb by drying. In such a physisorption process, it may be difficult to control the depth profile at nanometer-level resolutions. Therefore, we propose a new method that employs chemisorption instead of physisorption.

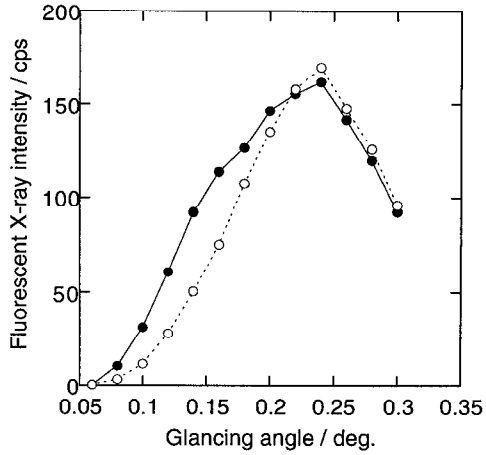

Fig. 2 Anglescan profiles of two spincoat samples (Ni, 5 x 10^{13} atoms cm^{-2}).

2-2. Proposal of a method of preparing standard samples

The proposed method is named "Immersion in Alkaline Hydrogen Peroxide solution" (IAP) [6, 7]. This method utilizes a mixed solution of ammonia, hydrogen peroxide, and water, which is a very common cleaning solution in semiconductor industry used to remove particles from silicon wafers [8]. If this solution contains metal ions, they are adsorbed onto the surface of the silicon wafer during the cleaning process [9]. This metal adsorption is known to be a major defect of this type of cleaning solution. However, we devised a method whereby we can make use of this adsorption phenomenon to make standard samples. In the IAP method, cleaned silicon wafers are immersed in the solution that is intentionally doped with a certain amount of metal ions such as Fe, Ni, and Zn. A schematic illustration of the reactions in the solution is shown in Fig. 3. At first, the hydrogen peroxide forms a thin layer of SiO_2, which is instantly etched by the ammonia. In all, these two reactions balance out, leaving about a 1-nm SiO_2 layer continuously during the immersion [10]. Based on chemical equilibrium, metal ions adsorb to the SiO_2 layer [11].

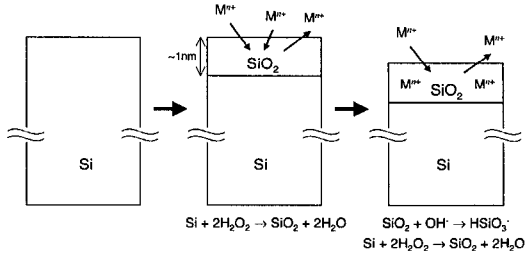

Fig. 3 Schematic models of surface reactions in alkaline hydrogen peroxide solution.

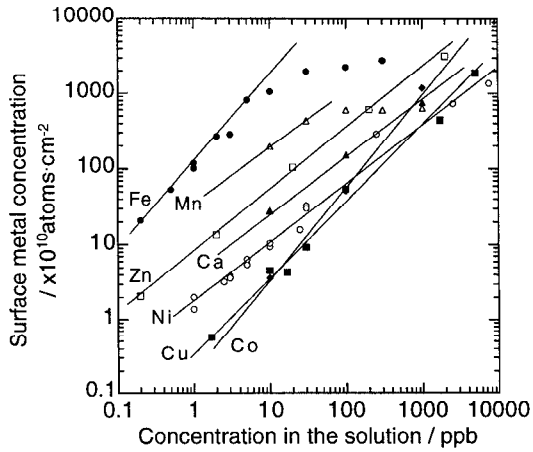

Fig. 4 Adsorption isotherms of several metals in 2.2M NH_4OH + 1.4M H_2O_2 solution at 80°C.

The "adsorption isotherms," the amount adsorbed versus the concentration of dissolved metal at a fixed temperature, are shown in Fig. 4 for several metals [7]. Here, the solution composition was

ISSN 1097-0002

2.2M ammonia and 1.4M hydrogen peroxide, the immersion time was 10 min., and the solution temperature was 80°C. The IAP method can be applied to these important elements in the range of at least 10^9 to 10^{13} atoms cm^{-2}. In addition, this method can also be applied to Al and Mg, although they are omitted here because they cannot be analyzed with ordinary TXRF. It should be mentioned, however, that alkaline metals (Na and K) and some heavy metals (Cr, W, and Ta) were not adsorbed.

We examined the reproducibility of the depth profiles by measuring the anglescans of the analyte elements on IAP wafers [6, 7]. Figure 5 compares the anglescans for IAP wafers that have different concentrations of Ni. The anglescans agreed well, which means that the depth profile is independent of the adsorbed concentration. Figure 6 compares the anglescans between three elements: Fe, Ni, and Zn. The results agreed well with each other, indicating that depth profile is independent of the element.

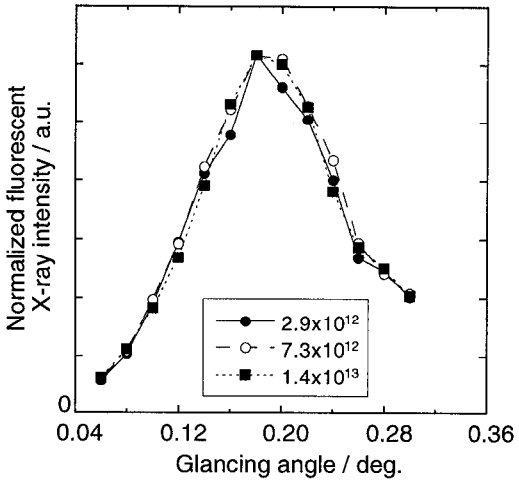

Fig. 5 Comparison of anglescan profiles for some IAP wafers with different concentrations of Ni.

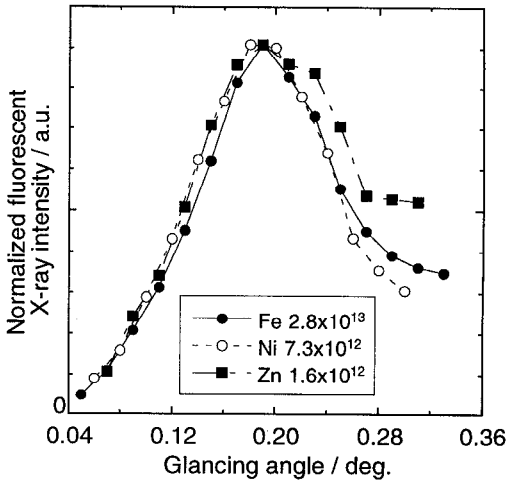

Fig. 6 Comparison of anglescan profiles for IAP wafers on which Fe, Ni, or Zn was adsorbed.

From a standpoint of use as a standard sample, uniformity of adsorption is also a critical factor. Table 1 shows the areal uniformity of metal adsorption evaluated by conducting 9-point TXRF mapping. The uniformity was typically 10% or less by relative standard deviation (RSD), which is comparable to that of traditional spincoat wafers

Table 1 Spatial uniformity of surface metal concentration for several IAP wafers.

Element	Adsorbed concentration / atoms·cm⁻²	Relative standard deviation / %
Fe	9.0×10^{11}	7.7
	4.5×10^{12}	3.5
	1.7×10^{13}	4.0
Ni	3.5×10^{11}	12.3
	3.3×10^{12}	19.6
	1.0×10^{13}	4.3
Zn	7.3×10^{11}	9.3
	3.0×10^{12}	3.4
	6.0×10^{12}	4.8

Table 2 Wafer-to-wafer uniformity of metal concentration for IAP wafers prepared in each single batch.

Element	Adsorbed concentration / atoms·cm⁻²	Relative standard deviation / %
Fe	4.5×10^{12}	0.96
Ni	1.6×10^{12}	5.9
Zn	3.0×10^{12}	5.4

ISSN 1097-0002

[4]. Table 2 lists the in-batch uniformity of adsorbed concentration. In this experiment, nine wafers were immersed in a single solution at one time, and the wafer-to-wafer uniformity was evaluated by analysis with TXRF or AAS. The dispersion was very small, less than ca. 6% by RSD. Good in-batch uniformity, as well as areal uniformity, is advantageous in standard or crosscheck samples for the contamination analysis of semiconductor surfaces.

The IAP wafers were actually used in a crosscheck experiment organized by the Ultra Clean Society (UCS) in Japan [12]. In this round-robin test, unidentified IAP samples were distributed to 14 participants, and each participant determined each sample by their own TXRF analysis. Initially, each machine was calibrated by applying individually prepared reference standard samples, but the result of the crosscheck was not satisfactory, as is shown in Fig. 7(a). The RSD was 56%, and the determination values ranged over factor of five. Another set of IAP wafers was then applied as common reference standard samples. Each participant drew a new calibration curve, and concentration of the unknown sample was recalculated. The results are shown in Fig. 7(b), in which the RSD improved more than factor of three. These results demonstrate that IAP wafers are suitable standard and crosscheck samples.

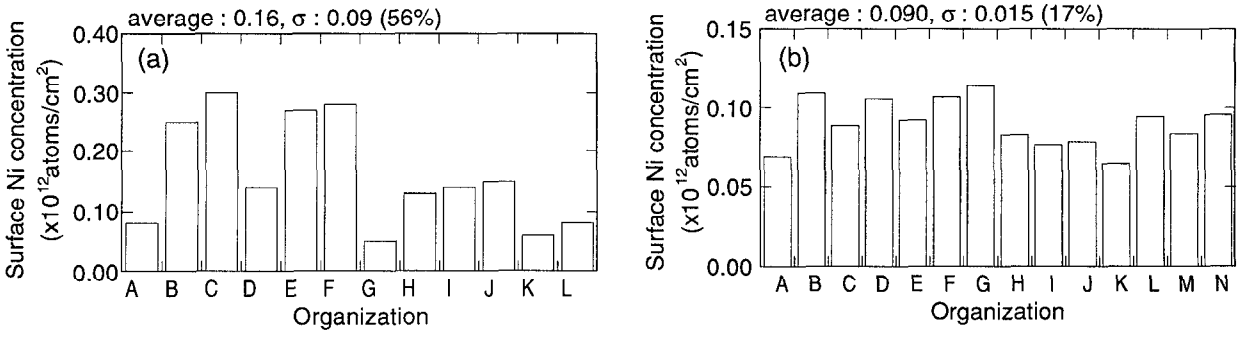

Fig. 7 TXRF round-robin test results organized by UCS [12]. (a) Reference standard sample was individually prepared by each participant, and (b) Common reference standard sample made with IAP was applied.

Although the practical limit on the number of IAP wafers made from a single solution was initially 25 (one-cassette capacity), the method was expanded to make 50 or more wafers [13]. Recently, IAP wafers were used as crosscheck standard samples in the international round-robin test of the VPD method organized by ISO/TC201/WG2.

3. IMPROVEMENTS IN TXRF INSTRUMENTS

As the design rule of LSI devices continually grow smaller, the contamination level of semiconductor surface has become stricter [14]. In order to analyze improvements in cleanliness, the Lower Limit of Detection (LLD) of TXRF had to be continuously improved. The LLD of TXRF is generally expressed by the following equation

$$LLD = 3\,\sigma_{BG}\,S, \qquad (1)$$

ISSN 1097-0002

where σ_{BG} represents the standard deviation of background intensity, and S is the slope of the calibration curve. In X-ray fluorescence, σ_{BG} can be replaced by $I_{BG}^{1/2}$, where I_{BG} is the background count of a blank sample. S can be substituted by C_{STD}/I_{STD}, where C_{STD} is the nominal concentration of a standard sample and I_{STD} is the intensity of fluorescent X-ray of a standard sample. Hence, eq 1 becomes

$$LLD = 3\, I_{BG}^{1/2}\, C_{STD}/I_{STD}. \qquad (2)$$

From this equation, we can recognize that there are two strategies to improve LLD: increasing I_{STD} or decreasing I_{BG}.

The initial effort was to increase I_{STD} by intensifying the primary X-ray. The introduction of an artificial high-reflectivity multilayer actually increased the primary X-ray intensity by several times than that of traditional single crystals such as LiF [15]. The intensification of the primary X-ray, however, is becoming impractical in recent TXRF machines for two reasons: increasing dead time of the detection system and impurity peaks caused by imperfections of the artificial multilayers [16]. Therefore, the next strategy for improving LLD should be the decrease of I_{BG}.

There are several factors that increase I_{BG}. We will consider three important factors: escape and scattering peaks, impurity peaks caused by imperfect monochromatizing, and diffraction by the substrate.

1) Escape and scattering peaks

The major excitation X-ray of semiconductor-oriented TXRF has been W-Lβ (9.67 keV), because of the achievable high intensity level. The W-Lβ source, however, brings two major interference problems: escape peak on Cu-Kα and scattering peak on Zn-Kα. The escape peak inevitably appears in energy-dispersive X-ray detection systems. The energy of the escape peak in W-Lβ excitation combined with a Si(Li) detection system is 7.93 keV, which is very close to Cu-Kα (8.04 keV), so that separating the small Cu-Kα from the escape peak is difficult. In addition, the shoulder of the large W-Lβ scattering overlaps Zn-Kα (8.63 keV), which makes separating the small Zn-Kα difficult. One way to avoid such interference is to replace W-Lβ with another excitation source; Au-Lβ (11.44 keV) may be one of the solutions [17]. Figure 8 compares the blank spectra of W-Lβ and Au-Lβ excitation. Since the escape peak in Au-Lβ excitation appears at 9.70 keV, no interference with Cu-Kα is observed. In addition, the Au-Lβ is well separated from Zn-Kα to avoid interference by the scattering X-ray.

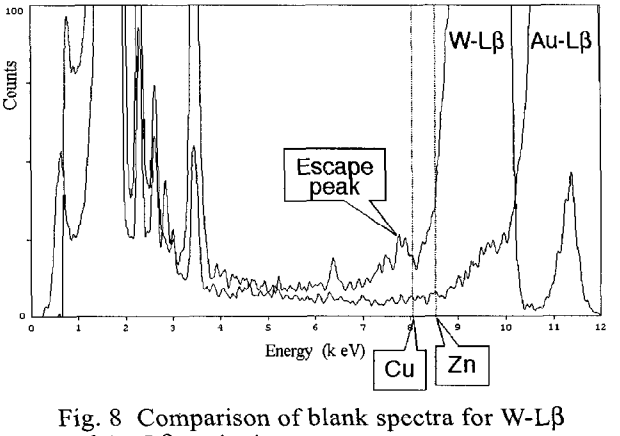

Fig. 8 Comparison of blank spectra for W-Lβ and Au-Lβ excitations.

ISSN 1097-0002

2) Impurity peaks caused by imperfect monochromatizing

Compared with traditional single crystals, an artificial multilayer is not a perfect monochromator; parts of white X-rays sometimes pass through to make impurity peaks in the spectrum. To reduce these impurity peaks, a dual-multilayer monochromator was proposed [16]. In this system, impurity X-rays are significantly reduced by application of the second monochromator, while the main characteristic X-rays are not greatly attenuated. Figure 9 compares the blank spectra of single- and dual-multilayer systems. Impurity peaks in the single-multilayer system at around 6 keV and 8.4 keV disappeared in the dual-multilayer system. In addition, as a secondary effect, the overall background level was lowered, probably because the overall incidence of white X-rays was reduced by the better monochromatizing.

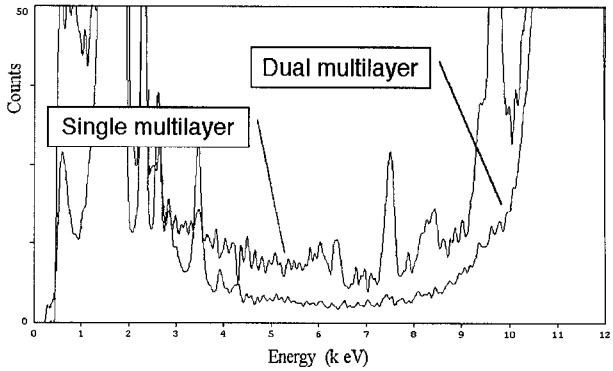

Fig. 9 Comparison of blank spectra for single- and dual-multilayer monochromators.

3) Diffraction

Since a silicon wafer is a single crystal, the diffraction of irradiated primary X-rays occurs at a certain azimuthal angle. The diffraction cannot be avoided in r-θ controlled stage because of the lack of a free axis [18, 19]. When diffraction occurs, the large diffraction peak increases the overall background level. To avoid the diffraction, an x-y-θ stage system was developed [16]. Because of the additional third axis, an arbitrary azimuthal angle can be set at any measurement spot on the sample, so the diffraction can be avoided.

By virtue of these improvements in instrumentation, state-of-the-art TXRF machines actually achieve an LLD of 2 x 10^9 atoms cm^{-2} [20].

4. PERFORMANCE OF CURRENT TXRF

By using IAP wafers as crosscheck standard samples, we tested the performance of current TXRF instruments near the LLD.

4-1. Experimental

Two types of TXRF machines were tested: W-Lβ and Au-Lβ excitations. Both employ rotating anodes (9 kW) and dual-multilayer monochromators. Both were TXRF300 models (Rigaku Industrial Corp., Japan) equipped with x-y-θ sample stages. The glancing angle was 0.06 deg. or 0.08 deg. for W-Lβ or Au-Lβ excitation, respectively. The integration time was 500 s per measuring spot. A 5-point mapping (center and half radius on the x- and y-axes) was conducted for each wafer at a fixed azimuthal angle.

ISSN 1097-0002

The crosscheck samples were prepared by using the IAP method previously described. The element tested was Cu. The targeted 5-level concentration ranged from blank to ca. 2 x 10^{10} atoms cm^{-2}. Their concentrations were separately determined with VPD-AAS, by using a VRC-300T (SES Corp., Japan) automatic VPD residue collector followed by a SIMAA6000 (PerkinElmer, Inc., MA) atomic absorption spectrophotometer.

4-2. Results

Figures 10 and 11 compare the W-Lβ and Au-Lβ excitation for Cu determination. In W-Lβ excitation, the linearity reaches to the level of 10^{9} atoms cm^{-2}, but the dispersion of 5-point mapping is

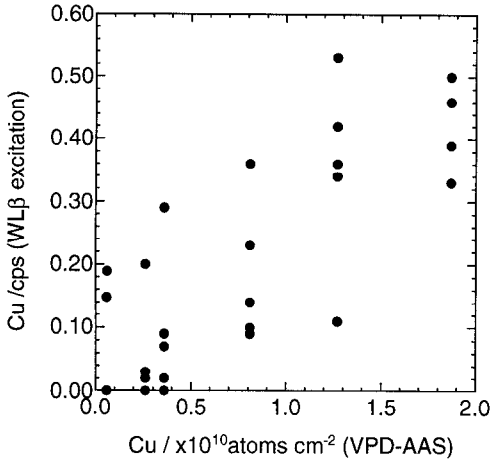

Fig. 10 Correlation of Cu between VPD-AAS and TXRF with W-Lβ excitation.

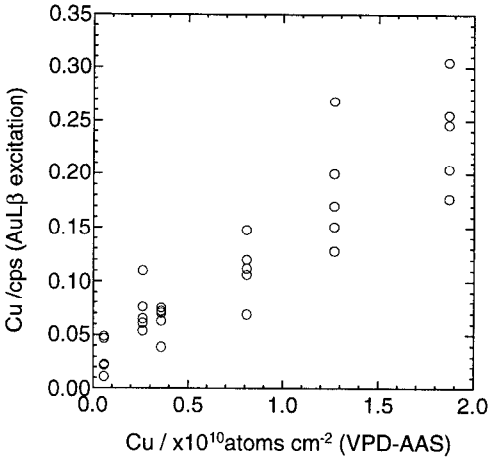

Fig. 11 Correlation of Cu between VPD-AAS and TXRF with Au-Lβ excitation.

large. The large dispersion may be due to interference caused by the escape peak. In comparison, in Au-Lβ excitation, although the signal intensity is around half that of W-Lβ excitation, the dispersion is very small even at the lower level of 10^{9} atoms cm^{-2}. For example, the RSD of Au-Lβ excitation for 0.26 x 10^{10} atoms cm^{-2} sample is 30.1%, while that of W-Lβ is 78.3%.

4-3. Actual application

For process characterization, we are actually using a TXRF machine equipped with an Au-Lβ excitation source. Since cleanliness of the silicon wafer manufacturing processes is strictly controlled, the wafers rarely sustain metallic contamination. However, un-

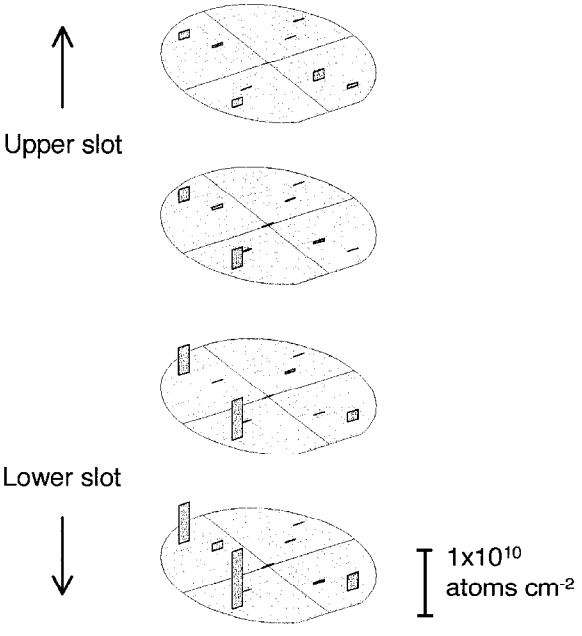

Fig. 12 Results of Cu mapping analysis by TXRF for four wafers sampled from a process.

ISSN 1097-0002

expected contamination does occur in rare instances. Figure 12 is an example of such contamination. Four wafers were sampled from a single wafer carrier treated by a certain process, then measured with TXRF. The results show that the left sides of the wafers are contaminated with low-level Cu, and that the contamination level highly related to the slot position in the wafer carrier. The level of Cu concentration at the contaminated spots is less than 1 x 10^{10} atoms cm^{-2}. Since the traditional wet technique (VPD-AAS etc.) is not able to analyze such a low-level localized contamination, the use of TXRF is advantageous to find causes of unexpected trace contaminants.

5. CONCLUSION

The application of TXRF for semiconductor process characterization was discussed. The depth profile of the analyte element plays a critical role in accurate determination by TXRF. To achieve reliable quantification, a method for preparing standard and crosscheck samples, named "IAP," was proposed. The method offers good level of reproducibility of depth profiles as well as areal and in-batch uniformity. Certain improvements of TXRF instruments were also discussed. The purity of the background spectra is critical in ultra-trace analysis, and improvements in instrumentation, such as Au-Lβ excitation, a dual-multilayer monochromator, and an x-y-θ stage actually reduced the background to help enable the identification of trace elements. We tested the performance of these recently improved TXRF instruments by analyzing IAP wafers intentionally contaminated with trace Cu, and demonstrated that a real-10^{9} atoms cm^{-2} analysis can actually be achieved.

ACKNOWLEDGMENTS

The author wishes to acknowledge Dr. T. Yamada (Rigaku Corp.), Mr. H. Kohno, and Mr. M. Matsuo (Rigaku Industrial Corp.) for kindly using their TXRF to measure our samples. The author also thanks Mr. T. Sakon, Dr. K. Shimanoe, Mr. K. Uemura, Mr. H. Arigane, Mr. S. Kawai, Mr. T. Matsunaga, Mr. M. Inamitsu, Mr. M. Yoshitomi, Mr. B. Shimomura, Mr. K. Okamoto, Mr. N. Tanaka, Mr. R. Udou, and Mr. T. Eguchi for their much suggestion and help with the experiments.

REFERENCES

[1] Fabry, L.; Pahlke, S.; Kotz, L.; Tölg, G., *Fresenius' J. Anal. Chem.*, **1994**, *349*, 260.

[2] Nishihagi, K.; Yamashita, N.; Fujino, N.; Taniguchi, K.; Ikeda, S., *Adv. X-Ray Anal.*, **1991**, *34*, 81.

[3] Mori, Y.; Uemura, K., *X-Ray Spectrom.*, **1999**, *28*, 421.

[4] Hourai, M.; Naridomi, T.; Oka, Y.; Murakami, K.; Sumita, S.; Fujino, N.; Shiraiwa, T., *Jpn. J. Appl. Phys.*, **1988**, *27*, L2361.

[5] Kondo, H.; Ryuta, J.; Morita, E.; Yoshimi, T.; Shimanuki, Y., *Jpn. J. Appl. Phys.*, **1992**, *31*, L11.

ISSN 1097-0002

[6] Mori, Y.; Shimanoe, K.; Sakon, T., *Anal. Sci.*, **1995**, *11*, 499.

[7] Mori, Y.; Shimanoe, K., *Anal. Sci.*, **1996**, *12*, 141.

[8] Kern, W.; Puotinen, D. A., *RCA Rev.*, **1970**, *31*, 187.

[9] Atsumi, J.; Ohtsuka, S.; Munehira, S.; Kajiyama, K., *Proceedings of the First International Symposium on Cleaning Technology in Semiconductor Device Manufacturing*, Hollywood, ECS Proceedings, *PV90-9*, **1990**, p.59.

[10] Sakurai, M.; Ryuta, J.; Morita, E.; Tanaka, K.; Yoshimi, T.; Shimanuki, Y., *Extended Abstracts of the 177th Electrochemical Society Meeting*, Montreal, ECS Proceedings, *PV90-1*, **1990**, p.710.

[11] Mori, Y.; Uemura, K.; Shimanoe, K.; Sakon, T., *J. Electrochem. Soc.*, **1995**, *142*, 3104.

[12] UC Standardization Committee, *Ultra Clean Technology*, **1996**, *8*, 44.

[13] Mori, Y.; Uemura, K., *Anal. Sci.*, **2000**, *16*, 987.

[14] "International Technology Roadmap for Semiconductors (ITRS)", http://public.itrs.net/Files/2000UpdateFinal/2kUdFinal.htm.

[15] Utaka, T.; Sako, Y.; Kohno, H.; Shoji, T.; Shimizu, K.; Miyazaki, K.; Shimazaki, A., *Adv. X-Ray Chem. Anal. Jpn.*, **1994**, *25*, 203.

[16] Funabashi, M.; Utaka, T.; Arai, T., *Spectrochim. Acta*, **1997**, *B52*, 887.

[17] Yamada, T.; Shoji, T.; Funabashi, M.; Utaka, T.; Arai, T.; Wilson, R., *Adv. X-Ray Chem. Anal. Jpn.*, **1995**, *26s*, 53.

[18] Yakushiji, K.; Ohkawa, S.; Yoshinaga, A.; Harada, J., *Jpn. J. Appl. Phys.*, **1992**, *31*, 2872.

[19] Yakushiji, K.; Ohkawa, S.; Yoshinaga, A.; Harada, J., *Jpn. J. Appl. Phys.*, **1993**, *32*, 1191.

[20] Yamada, T.; Matsuo, M.; Kohno, H.; Mori, Y., *Spectrochim. Acta B*, **2001**, *56*, 2307.